DOI: 10.1002/chem.201000600

Dumbbell-Shaped Dinuclear Iridium Complexes and Their Application to Light-Emitting Electrochemical Cells

Rubén D. Costa,[a] Gustavo Fernández,[b] Luis Sánchez,[b] Nazario Martín,*[b] Enrique Ortí,*[a] and Henk J. Bolink*[a]

Dedicated to Professor José Barluenga on the occasion of his 70th birthday

Abstract: A novel family of dumbbell-shaped dinuclear complexes in which an oligophenyleneethynylene spacer is linked to two heteroleptic iridium(III) complexes is presented. The synthesis, as well as the electrochemical and photophysical characterization of the new complexes, is reported. The experimental results are interpreted with the help of density functional theory calculations. From these studies we conclude that the lowest triplet excited state corresponds to a $^3\pi$–π^* state located on the conjugated spacer. The presence of this state below the ^{3}MLCT/^{3}LLCT emitting states of the end-capping Ir^{III} complexes explains the low quantum yields observed for the dinuclear complexes (one order-of-magnitude less) with respect to the mononuclear complexes. The potential application of the novel dinuclear complexes in optoelectronic devices has been tested by using them as the primary active component in double-layer light-emitting electrochemical cells (LECs). Although the luminance levels are low, the external quantum efficiency suggests that a near-quantitative internal electron-to-photon conversion occurs in the device. This indicates that the emission inside the device is highly optimized and that the self-quenching associated with the high concentration of the complex in the active layer is minimized.

Keywords: electroluminescence · iridium · light-emitting electrochemical cells · quenching pathways

Introduction

Multifunctional materials are designed to accomplish multiple performance objectives in a single system.[1] These objectives are usually related with optical, electrochemical, charge transport, and magnetic properties of the materials and with their integration into devices, such as organic photovoltaics (PVs) or organic light-emitting diodes (OLEDs).[2–9] A special type of building block for multifunctional materials is organometallic complexes and, more specifically, those complexes based on an iridium(III) metal core. Iridium complexes have been widely utilized in optoelectronics, owing to their relevant luminescent properties, such as high emission quantum yields, stability, long excited-state lifetimes, and easy tunability of the emission color.[10–14]

One of the most outstanding applications of ionic transition-metal complexes (iTMCs) is their use in the fabrication of a new type of solid-state electroluminescent devices, the so-called light-emitting electrochemical cells (LECs). LECs mainly consist of one active layer of a Ru^{II}- or Ir^{III}-based iTMC,[15,16] in which the charge of the iTMC is compensated with small mobile anions, such as hexafluorophosphate (PF_6^-). The presence of mobile ions leads to the formation of ionic junctions when an external electric field is applied, which lower the barriers for hole and electron injection and make LECs independent of the work function of the electrode material.[9,17–19] Therefore, air-stable electrodes, such as gold, silver, or aluminum, can be used in LECs, which makes its fabrication process cheaper and simpler compared to OLEDs.

[a] R. D. Costa, Prof. Dr. E. Ortí, Dr. H. J. Bolink
Instituto de Ciencia Molecular (ICMol)
Universidad de Valencia
P.O. Box 22085, 46071 Valencia (Spain)
Fax: (+34) 963543273
E-mail: enrique.orti@uv.es
henk.bolink@uv.es

[b] Dr. G. Fernández, Dr. L. Sánchez, Prof. Dr. N. Martín
Departamento de Química Orgánica
Facultad de Ciencias Químicas
Universidad Complutense, 28040 Madrid (Spain)
Fax: (+34) 913944103
E-mail: nazmar@quim.ucm.es

Supporting information for this article is available on the WWW under http://dx.doi.org/10.1002/chem.201000600.

 © 2010 Wiley-VCH Verlag GmbH & Co. KGaA, Weinheim View this journal online at wileyonlinelibrary.com

LEC devices showing high stabilities[20–23] and a wide range of emission colors, including white,[12,24–30] have been reported. However, moderate efficiencies are generally observed because of the high concentration of the iTMCs in the active layer that leads to an efficient self-quenching.[31,32] A useful strategy to enhance the efficiency of the device is to increase the distance between the iTMCs by attaching bulky groups in the periphery of the complexes.[25,32–35] This strategy, however, has an important limitation, as the iTMCs are responsible for all the processes, such as charge injection, charge transport by hopping, and emission. Therefore, if the distances between the ionic complexes in the active layer are greater than the hopping distances of the charge carriers, the LEC device does not work properly.[25,34]

We will show a plausible strategy to control the separation between the iTMCs by connecting two iridium(III) complexes by a π-conjugated spacer. Two novel dumbbell-shaped dinuclear iridium complexes (compounds **1a** and **1b** in Scheme 1) incorporating the oligophenyleneethynylene spacer endowed with two bipyridyl units (**6**) have been synthesized. The terminal bipyridyl units are used to link two heteroleptic iridium(III) moieties for which the coordination sphere is completed with two 2-phenylpyridine (ppy) (compound **1a**) or two 2-(2′,4′-difluorophenyl)pyridine (F_2ppy) cyclometalating ligands (compound **1b**). The electrochemical and photophysical properties measured for the novel dinuclear compounds are discussed with the help of density functional theory (DFT) calculations and in comparison with those obtained for the mononuclear Ir^{III} complexes [Ir(ppy)$_2$bpy][PF_6] (**8a**) and [Ir(F_2ppy)$_2$bpy][PF_6] (**8b**) (bpy = 2,2′-bipyridine) and the π-conjugated bridge **6**. The electroluminescence of LEC devices, built up using compounds **1a** and **1b** as the active components, is also presented and is rationalized in terms of the photophysical properties of the dumbbell-shaped dinuclear complexes.

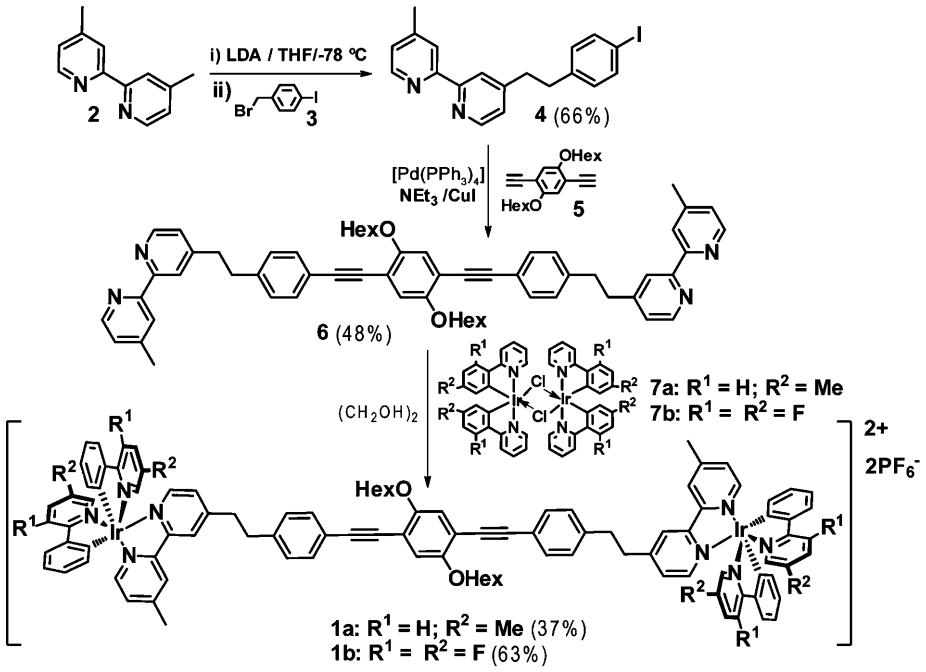

Scheme 1. Synthesis of the dumbbell-shaped dinuclear complexes.

Results and Discussion

Synthesis: The synthesis of the dinuclear complexes **1a** and **1b** was achieved by reacting the corresponding cyclometalated iridium chloro-bridged dimer **7**[36,37] with the π-conjugated spacer **6** in ethylene glycol under argon during 16 h. Compound **6** was prepared in a two-step synthetic procedure, starting from the nucleophilic substitution of the bromine atoms of commercially available 1-(bromomethyl)-4-iodobenzene (**3**) by the carbanion of dimethylbipyridine **2**, generated in situ upon addition of LDA at −78 °C. The subsequent twofold Sonogashira cross-coupling reaction between bipyridine **4** and 1,4-diethynyl-2,5-bis-(hexyloxy)benzene (**5**)[38] yields **6** in 48 %. All compounds were fully characterized through a variety of spectroscopic techniques (see the Experimental Section for details).

Electrochemical features: The electrochemical behavior of the dinuclear complexes **1a** and **1b** has been studied by cyclic voltammetry in dichloromethane at room temperature (Figure 1 and Table 1). Table 1 also includes the redox potentials measured for the bridge **6** and the mononuclear complexes **8a** and **8b**, which have been investigated as reference compounds.

The mononuclear complexes **8a** and **8b** present dissimilar oxidation behaviors. Although both complexes show a reversible first oxidation process, the potential at which this process appears is highly influenced by the presence of the fluorine atoms on the ppy ligands (Table 1). The fluorine substituents make complex **8b** (+1.58 V) a remarkably weaker reducing agent than complex **8a** (+1.12 V), and **8a** presents a second irreversible oxidation wave at +1.74 V that is not observed for **8b**. The electron-withdrawing effect of the fluorine atoms, therefore, increases the electrochemical E^1_{oxid}–E^1_{red} gap from 2.70 V in **8a** to 3.07 V in **8b**. In contrast to **8a** and **8b**, the two oxidation processes observed for the dinuclear complexes **1a** and **1b** remain mainly unaffected upon fluorine substitution

 © 2010 Wiley-VCH Verlag GmbH & Co. KGaA, Weinheim

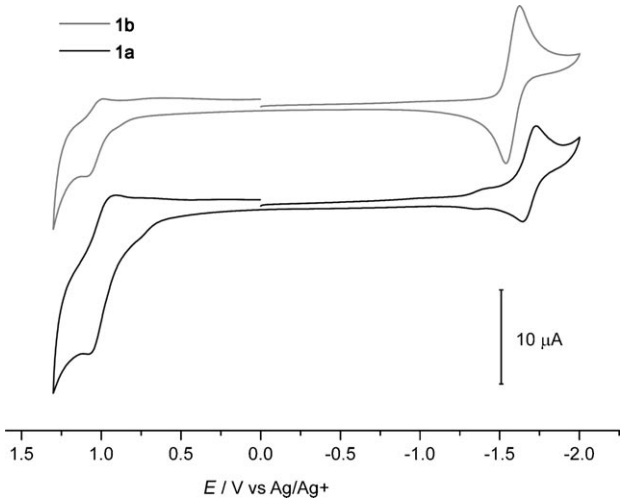

Figure 1. Cyclic voltammograms of the dinuclear complexes **1** measured in CH_2Cl_2 at room temperature (scan rate: 100 mV s^{-1}).

Table 1. Redox properties of the dinuclear complexes **1**, the spacer **6**, and the mononuclear complexes **8**.

Compound[a]	$E^1_{1/2\ red}$	$E^1_{1/2\ oxid}$	E^2_{oxid}[b]
1a	−1.67	+0.99	+1.73
1b	−1.58	+1.06	+1.70
6	−1.81[c]	+1.00	+1.50
8a	−1.58	+1.12	+1.74
8b	−1.49	+1.58	–

[a] V versus Ag/Ag^+, CH_2Cl_2 as solvent, GCE as working electrode, Pt as counter-electrode, Bu_4NClO_4 (0.1 M) as supporting electrolyte; scan rate 100 mV s^{-1}. [b] Very broad and irreversible wave. [c] Very weak and irreversible wave.

(Table 1) and no appreciable increase of the electrochemical gap is detected (**1a**: 2.66 V, **1b**: 2.64 V). These results suggest that oxidation in complexes **1a** and **1b** does not take place on the end-capping iTMCs and should involve the π-conjugated spacer. Indeed, oxidation of **6** (+1.00 V) occurs at similar potentials than in **1a** (+0.99 V) and **1b** **(+1.06 V).**

Ground-state molecular and electronic structures: The molecular and electronic structures of the dinuclear complexes **1**, the π-conjugated spacer **6**, and the mononuclear complexes **8** were investigated by performing DFT calculations at the B3LYP/(6-31G**+LANL2DZ) level. To simplify the calculations the hexyloxy groups of the wire were removed and all the molecules were fully optimized within C_2 symmetry constraints (the Computational Details are described in the Experimental Section).

The molecular structures calculated for compounds **1** are almost identical to those obtained for the central bridge and the mononuclear complexes **8**. In Table 2 the values computed for selected bond lengths of the end-capping iTMCs of compounds **1** are collected, they show a near octahedral coordination of the Ir^{III} metal. The $Ir-C_{ppy}$ and $Ir-N_{bpy}$ bond lengths shorten by 0.022 and 0.008 Å, respectively, in passing

Table 2. Selected bond lengths (in Å) calculated for complexes **8** and **1**.

Selected bonds	**8a**	**8b**	**1a**	**1b**
$Ir-C_{ppy}$	2.024	2.002	2.023	2.002
$Ir-N_{ppy}$	2.083	2.083	2.083	2.083
$Ir-N_{bpy}$	2.218	2.210	2.219	2.205

from **1a** to **1b** and evidence the contraction effect that the electron-withdrawing fluorine groups attached to the ppy ligands have on the coordination sphere of the metal. A similar contraction is computed for **8a** and **8b**. As expected, the fluorine groups do not affect the structure of the wire in compounds **1**. The central part of the wire consists of a π-conjugated structure with phenyl rings connected by ethynylene groups (C−C and C≡C bonds of 1.42 and 1.22 Å, respectively). The oligophenyleneethynylene spacer is linked to the iTMC moieties by saturated ethylene bridges (C−C bonds of 1.55 Å).

Displayed in Figure 2 are the electronic density contours calculated for the HOMOs and the LUMOs of **1a**, together with those obtained for the mononuclear complex **8a** and

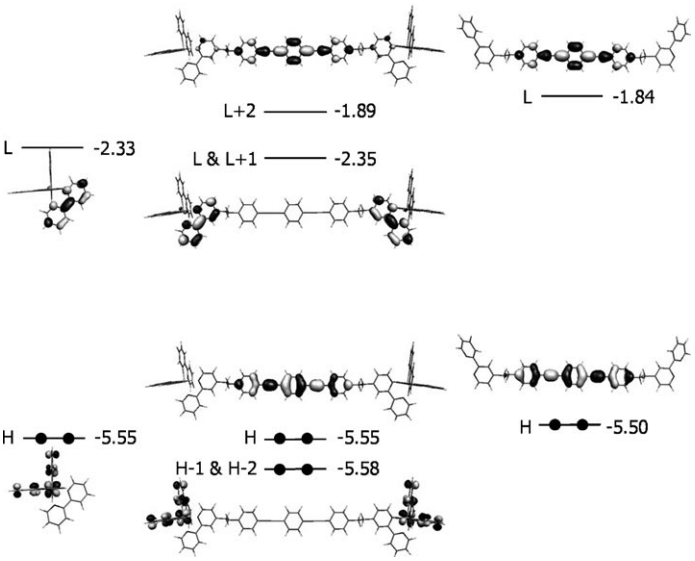

Figure 2. Schematic diagram showing the electronic density contours (0.03 e bohr^{-3}) and energies (in eV) calculated for the frontier molecular orbitals of the mononuclear complex **8a** (left), the dinuclear complex **1a** (center), and the central bridge **6** (right). H and L denote HOMO and LUMO, respectively. Molecular orbital energies correspond to those calculated in acetonitrile solution.

the spacer **6**. The HOMO of **8a** is composed of a mixture of iridium dπ orbitals (t_{2g}) and phenyl π orbitals distributed equally among the two ppy ligands, whereas the LUMO resides on the bpy ligand (see Figure 2, left). As the fluorine groups in **8b** are introduced on the phenyl rings of the ppy ligands, their electron-withdrawing effect stabilizes the HOMO (−5.96 eV) in a higher degree than the LUMO (−2.44 eV) with respect to the frontier molecular orbitals of

 © 2010 Wiley-VCH Verlag GmbH & Co. KGaA, Weinheim

complex **8a**. The relative stabilizations of the HOMO (0.41 eV) and the LUMO (0.11 eV) justify the higher oxidation potential (+0.46 V) and the lower reduction potential (+0.09 V) measured for **8b** in comparison to those obtained for **8a** (see Table 1). The HOMO–LUMO energy gap increases by 0.30 eV in passing from **8a** to **8b** in good agreement with the increase experimentally measured for the electrochemical E^1_{oxid}–E^1_{red} gap (0.37 V).

Calculations show that the LUMO and LUMO+1 in compounds **1** reside on the bpy ligands and correspond to the in-phase and out-of-phase combination of the LUMOs of the mononuclear complexes (Figure 2, centre). They are degenerate and appear at slightly lower energies for **1b** (−2.42 eV) than for **1a** (−2.35 eV), as is found for **8b** and **8a** and in agreement with the lower reduction potential measured for **1b**. The LUMO of the wire appears as the LUMO+2 and is calculated 0.46 (**1a**) and 0.51 eV (**1b**) higher in energy. In contrast to the LUMO, the HOMO in compounds **1** is found to be located on the conjugated part of the wire and corresponds to the π-HOMO of **6**. This explains the similar oxidation potentials recorded for compounds **1** (Table 1), as fluorine substitution has no significant effect on the wire and the energy of the HOMO remains mostly unaffected (**1a**: −5.55 eV, **1b**: −5.58 eV). The calculations support that reduction takes place on the bpy ligands of the end-capping iTMCs, whereas the oxidation implies the conjugated spacer. This determines that, in contrast with what is found for complexes **8a** and **8b**, the HOMO–LUMO gap in compounds **1** remains mainly constant (3.2 eV), in agreement with the electrochemical measurements. The electronic properties calculated for the dinuclear complexes **1** suggest that the electronic communication between the end-capping iTMCs and the central conjugated structure of the spacer is rather weak.

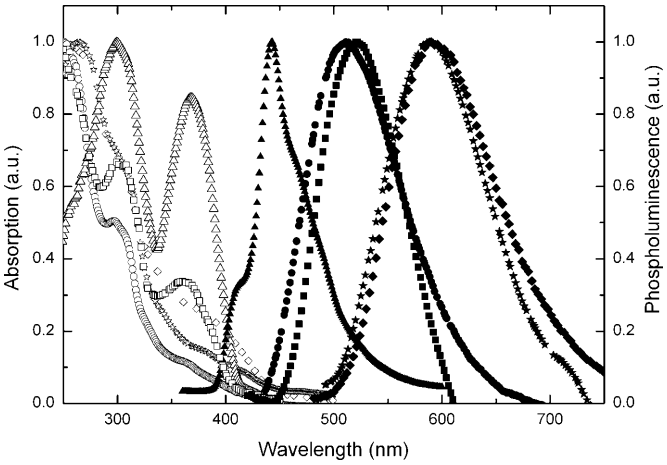

Figure 3. Absorption (open symbols) and photoluminescence (full symbols) spectra of Ir^{III} complexes **1a** (diamonds), **8a** (stars), **1b** (squares), and **8b** (circles) in de-aerated acetonitrile ($\approx 10^{-6}$ M) and of the central spacer **6** (black triangles) in *o*-dichlorobenzene ($\approx 10^{-6}$ M).

Table 3. Photophysical properties of the dinuclear complexes **1**, the π-conjugated spacer **6**, and the mononuclear complexes **8**.

Compound	Absorption	Emission	Decay Dynamics[c]			
	λ_{max} [nm][a]	λ_{max} [nm][a]	ϕ_r[a]	τ [μs][a]	k_r [s^{-1}]	k_{nr} [s^{-1}]
1a	217, 270, 372	588	9×10^{-3}	0.4	2.3×10^{4}	2.8×10^{6}
1b	245, 305, 363	521	7×10^{-3}	1.2	0.6×10^{4}	8.5×10^{5}
6	294, 367[b]	443[b]	0.84[b]	3.0×10^{-3}[b]	2.8×10^{8}	5.3×10^{7}
8a	222, 270	589	0.14	0.6	2.3×10^{5}	1.4×10^{6}
8b	250, 296	512	0.18	1.7	1.1×10^{5}	5.0×10^{5}

[a] Measured in nitrogen-saturated acetonitrile (298 K, $\approx 10^{-6}$ M). [b] Measured in nitrogen-saturated *o*-DCB (298 K, $\approx 10^{-6}$ M). [c] $\lambda_{exc}=310$ nm, ϕ_r and τ are ±10%.

Photophysical properties and excited electronic states: Displayed in Figure 3 are the absorption and photoluminescence spectra recorded for the dinuclear complexes **1** together with those registered for the mononuclear complexes **8** and the π-conjugated spacer **6**. Summarized in Table 3 are the absorption and emission properties. Compound **6** exhibits two intense absorption bands at $\lambda=294$ and 367 nm that are assigned to the π–π* excitations of the central oligophenyleneethynylene spacer on the basis of time-dependent DFT (TD-DFT) calculations performed for **6** by using the ground-state optimized structure. The absorption bands observed for compound **1** in the high-energy region ($\lambda=250$–300 nm) correlate with the bands recorded for the mononuclear complexes **8**. These bands are attributed to singlet spin-allowed ligand-centered (^{1}LC) transitions that imply the phenylpyridine and the bipyridine ligands.[11,12] Some contribution of the oligophenyleneethynylene spacer is also observed in this region for compound **1b**. The low-intensity bands that complexes **8** present in the $\lambda=350$–400 nm region, which are associated with the metal-to-ligand charge transfer (^{1}MLCT) transitions, are reinforced for the dinuclear complexes by the π–π* absorptions of the conjugated spacer and a better-defined band emerges at $\lambda\approx370$ nm for **1a** and **1b**.

The photoluminescence of **6** is characterized by a poor-resolved structured band with maximum emission at $\lambda=$ 443 nm (Figure 3). It corresponds to an efficient fluorescence process with a high quantum yield ($\phi_r=0.84$) and a short excited-state lifetime ($\tau=3$ ns). In contrast, the photoluminescence of compounds **1** is described as a broad structureless band centered at $\lambda=588$ nm (2.11 eV) and $\lambda=$ 521 nm (2.38 eV) for **1a** and **1b**, respectively. The shape of the bands and the emission maxima recorded for compounds **1** agree perfectly with those obtained for the respective mononuclear complexes **8a** and **8b** (see Figure 3 and Table 3). The emission maximum blue-shifts in going from **8a** to **8b** by 77 nm as it is also observed for **1a** and **1b**. Therefore, the nature of the emitting excited state should be

 © 2010 Wiley-VCH Verlag GmbH & Co. KGaA, Weinheim

the same and the emission of compounds **1** can be clearly ascribed to the phosphorescence of the end-capping iTMCs.

The mononuclear complexes **8** show a strong phosphorescence emission with moderate quantum yields (**8a**: 0.14, **8b**: 0.18) and long excited-state lifetimes in the μs scale. In contrast, compounds **1** present very low quantum yields (**1a**: 9×10^{-3}, **1b**: 7×10^{-3}), whereas the excited-state lifetimes have similar values (see Table 3). The photophysical parameters obtained for compounds **1** yield radiative-rate constants one order-of-magnitude lower than those determined for the mononuclear complexes and non-radiative-rate constants that approximately double those calculated for **8**. This photophysical behavior suggests that compounds **1** should present an additional non-radiative deactivation pathway compared with complexes **8**. To investigate the origin of the deactivation pathway, transient absorption experiments in the μs time domain were performed in combination with DFT calculations.

The transient absorption spectra recorded for **1a** and **8a** are compared in Figure 4 (Figure S1 in the Supporting Information shows those recorded for **1b** and **8b**). Instantaneous formation of broad stimulated emission features are observed at $\lambda=600$ and 520 nm for the mononuclear complexes **8a** and **8b**, respectively. Their decay kinetics are adequately fitted to mono-exponential decays with lifetimes of 0.6 (**8a**) and 1.7 μs (**8b**) and are assigned to the decay of the lowest triplet state. Similar transient absorption spectra have been observed for other ionic ruthenium and iridium complexes.[36,37] DFT calculations including full-geometry optimization show that the lowest-energy triplet state of compounds **8a** and **8b** result from the monoelectronic HOMO→LUMO excitation and implies a mixing of metal-to-ligand and ligand-to-ligand charge transfer (^{3}MLCT/^{3}LLCT). This mixed nature is confirmed by the spin-density distribution calculated for **8a** (Figure 5) that perfectly matches the electronic distribution of the HOMO and the LUMO.

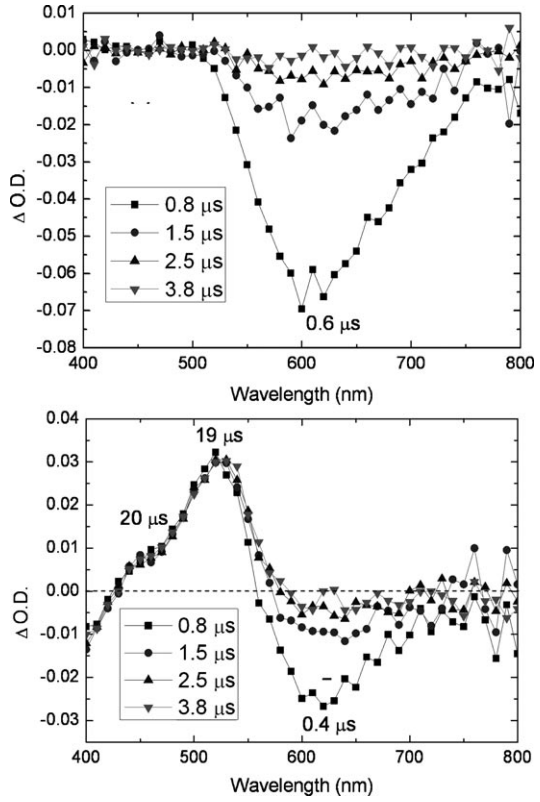

Figure 4. Transition difference spectra obtained by means of laser flash-photolysis experiments at $\lambda=310$ nm in degassed acetonitrile solutions at room temperature with low concentration (10^{-6} M) of complex **8a** (top) and compound **1a** (bottom).

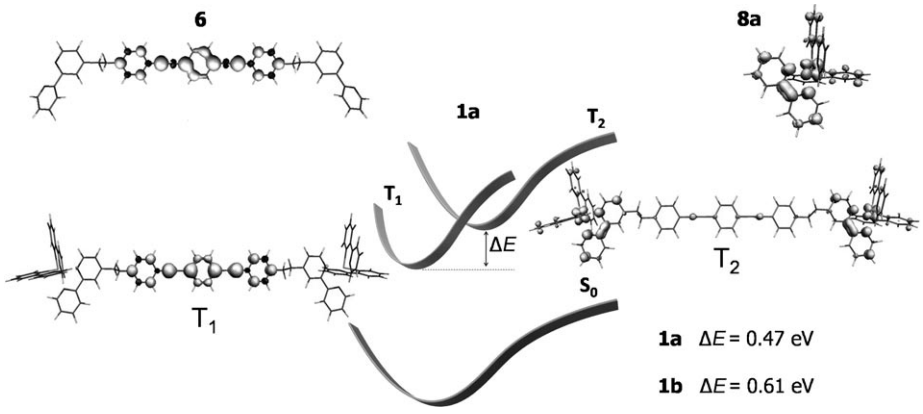

Figure 5. Schematic energy diagram showing the adiabatic energy difference between the T_1 and T_2 states (ΔE) calculated for compounds **1a** and **1b**. The electronic nature of the excited states is illustrated by the spin density contours (0.05 e bohr^{-3}) calculated for the T_1 and T_2 states of **1a**. The spin density of the lowest triplet of the free ligand **6** (top, left) and the mononuclear complex **8a** (top, right) are included for comparison purposes

The transient absorption spectrum of **1a** presents new features if compared with that of **8a** (Figure 4). Photoexcitation of compound **1a** leads to μs transient signals that include a broad stimulated emission at $\lambda=600$ nm with mono-exponential decay of 0.4 μs and absorption bands centered at $\lambda=445$ and 520 nm. In compound **1b**, the stimulated emission appears in the same region that the positive absorption band at $\lambda=520$ nm and only a low-intensity absorption band is observed (see Figure S1 in the Supporting Information). For compound **1a**, the position of the stimulated emission ($\lambda=$ 600 nm) and the fitted decay lifetime (0.4 μs) confirm that the emitting triplet state is the same than in **8a** ($\lambda=600$ nm, 0.6 μs). The absorption bands are fitted to a long mono-exponential decay of around 19 μs for both **1a** and **1b**. These absorption bands are not observed for the mononuclear

 © 2010 Wiley-VCH Verlag GmbH & Co. KGaA, Weinheim

complexes and they should be ascribed to the excitation of a low-energy triplet state that involves the spacer.

To describe the triplet excited-state manifold of compounds **1**, time-dependent DFT (TD-DFT) calculations were performed for **1a** and **1b** on the ground-state fully-optimized geometries. For both compounds, the lowest-energy triplet state (T_1, ^3B) results from the monoelectronic HOMO→LUMO+2 excitation that only implies the wire and corresponds to the $^3\pi$–π^* HOMO→LUMO transition of the oligophenyleneethynylene spacer (see Figure 2). The next two triplets, T_2 (^3A) and T_3 (^3B), are degenerate and originate in the transitions from the HOMO−1 and HOMO−2 to the LUMO and LUMO+1. These states correspond to the lowest-energy ^{3}MLCT/^{3}LLCT triplet of the mononuclear complexes. T_1 is calculated at 2.26 eV above the ground state and is separated from T_2 and T_3 by 0.20 (**1a**) and 0.56 eV (**1b**). TD-DFT calculations therefore suggest that the lowest-energy triplet of the dinuclear complexes **1** is the $^3\pi$–π^* state of the wire.

To further investigate the nature of the lowest-energy triplet state, the geometries of the T_1 and T_2 states of compounds **1** were optimized under C_2 symmetry restrictions. After full-geometry relaxation, the $^3\pi$–π^* triplet of the wire continue to be the most stable and is calculated to lie 0.47 (**1a**) and 0.61 eV (**1b**) below the ^{3}MLCT/^{3}LLCT triplets of the end-capping iTMCs compounds. The nature of T_1 and T_2 is confirmed by the spin-density distributions shown in Figure 5, which perfectly correlate with the spin densities calculated for the lowest triplet state of the π-conjugated central bridge and of the mononuclear complex, respectively. Theoretical calculations, therefore, suggest that the absorption bands observed in the transient absorption spectra of compounds **1** result from the excitation of the lowest triplet state (T_1) centered on the wire. The presence of the $^3\pi$–π^* triplet below the emitting states centered on the iTMCs depopulates these states and explains the lower photoluminescence quantum yield observed for compounds **1** compared with complexes **8**.

Electroluminescence properties: Simple two-layer LECs were built by using the dinuclear complexes **1a** and **1b**. The details concerning the device fabrication are described in the Experimental Section. Upon applying a bias of 3 V, the build up of the luminance is synchronous with that of the current density (see Figure S2 in the Supporting Information). The observed time-delayed response is a typical feature of LECs and reflects the mechanism of device operation for which the PF_6^- counter-ions have to reach the interface of the electrodes which enhances the charge-injection process.[15,16]

The electroluminescence (EL) spectra of compounds **1** consist of a broad structureless band with a shape similar to the photoluminescence spectra recorded in solution (Figure 6). As expected, compound **1a** emits in the yellow region (CIE coordinates: $x=0.4527$; $y=0.4164$) with a maximum at $\lambda=596$ nm, whereas **1b** emits in the green region ($x=0.3696$; $y=0.4625$) with a maximum at $\lambda=540$ nm.[38]

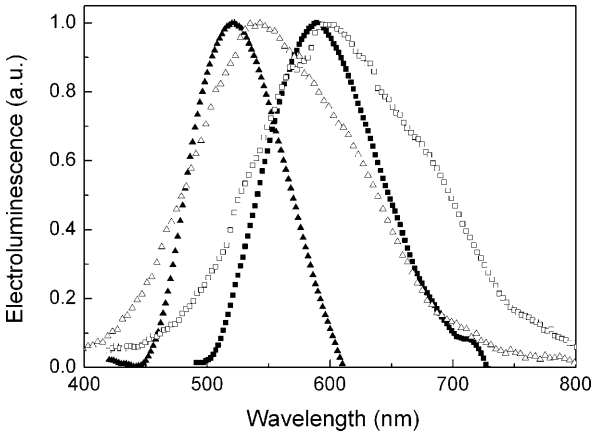

Figure 6. Photoluminescence (full symbols) in acetonitrile and electroluminescence (open symbols) spectra of compounds **1a** (squares) and **1b** (triangles). The electroluminescence spectra are recorded at a constant voltage of 3 V.

The EL maxima are red-shifted by 10–20 nm, with respect to the photoluminescence maxima, which is often observed in LECs.[15,16]

LEC devices based on compounds **1** show low emission levels with luminance maxima below 10 cd m^{-2}. The low luminance values result from the low emission quantum yield observed for compounds **1**, owing to the quenching of the phosphorescence of Ir^{III} complexes by the $^3\pi$–π^* state of the conjugated spacer. Although the luminance level is low, the external quantum efficiency (EQE) values obtained for LECs based on **1a** (0.16%) and **1b** (0.13%) are rather close to the maximum EQE values (**1a**: 0.20%, **1b**: 0.16%) estimated from the photoluminescence quantum yields.[39,40] This indicates that emission inside the device is highly optimized, as it is nearly as efficient as we can expect from the photophysical properties of **1a** and **1b**, and suggests that the self-quenching due to the high iTMC concentration in the device has been minimized. To obtain higher luminances, the low $^3\pi$–π^* state of the π-conjugated bridge linking the Ir^{III} complexes should be shifted to energies above the emitting ^{3}MLCT/^{3}LLCT iTMC triplets. This will suppress the undesired non-radiative deactivation pathway through the wire and LEC devices with high luminances can be expected.

Conclusion

The synthesis and the electrochemical, photophysical, and theoretical characterization of a novel family of dumbbell-shaped dinuclear complexes (**1**), in which an oligophenyleneethynylene spacer is linked with two heteroleptic iridium(III) complexes, have been reported. From these studies we conclude that the lowest triplet excited state in the new complexes corresponds to a $^3\pi$–π^* state located on the conjugated spacer. The appearance of this state below the ^{3}MLCT/^{3}LLCT emitting states of the end-capping Ir^{III} complexes is an efficient quenching pathway, which explains the

 © 2010 Wiley-VCH Verlag GmbH & Co. KGaA, Weinheim

low quantum yields observed for the dinuclear complexes in comparison with the mononuclear Ir^{III} complexes. Although complexes **1** present poor photophysical properties, their application in optoelectronic devices has been tested by using them as the primary active component in double-layer light-emitting electrochemical cells (LECs). Electroluminescence emission in the green and yellow regions is obtained under applying an external voltage of 3 V. The EQE values obtained for the devices are almost the same that the maximum EQE values estimated from the photoluminescence quantum yields of the complexes. This suggests that a near-quantitative internal electron-to-photon conversion occurs and that emission inside the device is highly optimized. The introduction of a molecular spacer to control the separation of the iTMCs in the active layer is, therefore, a useful strategy to minimize the self-quenching in the operating device. The design of new dinuclear Ir^{III} complexes connected by π-conjugated spacers that do not act as quenchers of the phosphorescent emission is of high interest for production of highly-efficient LECs.

Experimental Section

Materials and solvents: All solvents were dried according to standard procedures. Reagents were used as purchased. All air-sensitive reactions were carried out under an argon atmosphere.

Synthesis and characterization: Flash chromatography was performed by using silica gel (Merck, Kieselgel 60, 230–240 mesh or Scharlau 60, 230–240 mesh). Analytical thin layer chromatography (TLC) was performed by using aluminum coated Merck Kieselgel 60 F254 plates. The NMR spectra were recorded by using a Bruker Avance 300 (^{1}H: 300 MHz; ^{13}C: 75 MHz) and a Bruker Avance III 700 MHz spectrometer at 298 K using partially deuterated solvents as internal standards. Coupling constants (J) are denoted in Hz and chemical shifts (δ) in ppm. Multiplicities are denoted as follows: s = singlet, d = doublet, t = triplet, m = multiplet, br = broad.

Compound **5**,[41] the cyclometalated iridium chloro-bridged dimer **7**,[42,43] and compounds **8**[11] were prepared according to previously reported synthetic procedures and showed identical spectroscopic properties to those reported therein.

Compound 4: 4-Methyl-2-(4-methylpyridin-2-yl)pyridine (**2**, 4.03 g, 21.9 mmol) in dry THF was added dropwise to a freshly prepared lithium diisopropylamide (LDA, 2.3 g, 23.07 mmol) at −78 °C and under an argon atmosphere. The resulting solution was stirred in these conditions for one hour. After that, this solution was added through a cannula to a solution of 1-(bromomethyl)-4-iodobenzene (**3**, 5 g, 16.84 mmol) in dry THF (50 mL). The solution was stirred in these conditions overnight allowing it to reach room temperature. After that, methanol (20 mL) was added. After evaporation of the solvent under reduced pressure, the residue was washed with water, extracted with methylene chloride and dried over $MgSO_4$. After evaporation of the solvent, the residue was purified by column chromatography (silica gel, chloroform/ethanol (100/1)) yielding compound **4** as a white solid. (4.5 g, 66 %). ^{1}H NMR ($CDCl_3$, 300 MHz): δ = 8.55 (d, J = 1.5 Hz, 2H; H_g+$H_{g'}$), 8.25 (d, J = 1.5 Hz, 2H; H_f+$H_{f'}$), 7.60 (d, J = 9 Hz, 2H; H_a), 7.15 (d, J = 1.5 Hz, 1H; H_e), 7.13 (d, J = 1.5 Hz, 1H; $H_{e'}$), 6.92 (d, J = 9 Hz, 2H; H_b), 2.97 (m, 4H; H_c+H_d), 2.45 ppm (s, 3H; H_i); ^{13}C NMR ($CDCl_3$, 75 MHz): δ = 156.8, 156.4, 151.4, 149.5, 149.3, 148.4, 140.9, 137.9, 130.8, 125.1, 124.2, 12.4, 121.5, 91.6, 37.4, 36.5, 21.5 ppm; FTIR (neat): $\tilde{\nu}$ = 3052, 2928, 2860, 2208, 1727, 1595, 1554, 1515, 1461, 1414, 1380, 1276, 1212, 1116, 1019, 941, 895, 827, 761, 723, 694 cm^{-1}; ESI-MS: m/z: [M^+] = 400.

Compound 6: Compounds **4** (1.34 g, 3.37 mmol) and **5** (0.5 g, 1.53 mmol) were dissolved in dry THF (25 mL) under argon atmosphere and diisopropylamine (1.3 mL), tetrakis(triphenylphosphine)palladium(0) (0.17 g, 0.15 mmol) and copper(I) iodide (0.03 g, 0.15 mmol) were added. The reaction mixture was heated at 50 °C and stirred overnight. After evaporation of the solvent under reduced pressure, the residue was washed with NH_4Cl, extracted with methylene chloride and dried over $MgSO_4$. After evaporation of the solvent, the residue was purified by column chromatography (silica gel, chloroform/ethanol (200:1) yielding **6** as a yellowish solid (0.50 g, 48 %). ^{1}H NMR ($CDCl_3$, 300 MHz): δ = 8.55 (d, J = 1.5 Hz, 4H; H_g+$H_{g'}$), 8.30 (d, J = 1.5 Hz, 4H; H_f+$H_{f'}$), 7.47 (d, J = 9 Hz, 4H; H_a), 7.15 (d, J = 9 Hz, 4H; H_b), 7.14 (d, J = 1.5 Hz, 4H; H_e), 7.08 (d, J = 1.5 Hz, 4H; $H_{e'}$), 7.01 (s, 2H; H_j), 4.03 (t, J = 9 Hz, 4H; H_k), 3.02 (m, 8H; H_c+H_d), 2.45 (s, 2H; H_j), 1.85 (m, 4H), 1.54 (m, 4H), 1.38 (m, 4H), 0.92 ppm (t, J = 9 Hz, 6H); ^{13}C NMR ($CDCl_3$, 75MHz): δ = 159.5, 133.8, 133.5, 124.6, 115.5, 115.1, 90.8, 87.2, 72.3, 71.2, 71.1, 71.0, 70.0, 67.9, 59.5 ppm; FTIR (neat): $\tilde{\nu}$ = 3050, 3014, 2927, 2958, 1927, 1624, 1594, 1554, 1482, 1456, 1376, 1247, 1195, 1107, 1062, 900, 822, 765, 707 cm^{-1}; ESI-MS: m/z: [M^+] = 870.

General procedure for the heteroleptic iridium(III) complexes (1): Complexes **1** were synthesized by mixing of starting iridium complexes **7** (**7a**: 0.0564 g, 0.05 mmol; **7b**: 0.0608 g, 0.05 mmol) and spacer **6** (0.04 g, 0.055 mmol) in an ethyleneglycol solution heated to reflux during 16 h. Upon cooling to room temperature, the resulting yellow mixture was transferred to a separation funnel with water (40 mL) and washed with diethyl ether (3 × 30 mL). A concentrated solution of ammonium hexafluorophosphate (1 g) in water (10 mL) was slowly added, at 0 °C, to the reaction mixture, yielding a colored suspension. The compound was transferred to the fridge for 16 h and the precipitate was collected by filtration. The yellow product was recrystallized from acetonitrile/diethyl ether.

Complex 1a: Yield: 37 %. ^{1}H NMR (CD_2Cl_2, 700 MHz): δ = 8.49–8.43 (m, 4H); 7.8–7.82 (m, 4H); 7.71 (d, J = 5.1 Hz, 6H); 7.54 (m, 4H); 7.47–7.39 (m, 6H); 7.17–7.09 (m, 9H); 6.98–6.96 (m, 6H); 6.85–6.82 (m, 4H); 6.08 (s, 4H); 3.12–3.04 (m, 8H); 2.60 (s, 6H; Mebpy); 2.13 (s, 12H; Meppy);1.56–0.88 ppm (m, 26H); ^{13}C NMR ($CDCl_3$, 175 MHz): δ = 167.86, 160.38, 155.30, 154.97, 150.53, 150.01, 148.27, 141.00, 137.75, 132.33, 129.31, 128.90, 128.72, 128.54, 128.31, 128.17, 128.14, 126.60, 124.77, 124.48, 123.57, 123.50, 122.54, 121.38, 119.37, 119.30, 119.06, 77.53, 41.08, 36.74, 35.75, 31.56, 29.69, 29.36, 29.28, 25.69, 22.64, 21.31, 13.82 ppm; ESI-MS: m/z: [M^{+2}] = 966.

Complex 1b: Yield, 63 %.^{1}H NMR ($CDCl_3$, 700 MHz): δ = 8.37 (m, 4H; z), 7.88 (m, 4H), 7.52 (d, J = 7.5 Hz, 4H), 7.48 (d, J = 7.5 Hz, 4H), 7.36 (s, 4H), 7.34 (d, J = 7.5 Hz, 4H), 7.29 (d, J = 7.5 Hz, 4H), 7.24 (d, J = 7.5 Hz, 4H), 7.10 (s, br, 4H), 7.06 (s, 4H), 6.65 (t, J = 11.9 Hz, 4H), 5.78 (dd, J_1 = 2 Hz, 4H), 4.07 (t, J = 9 Hz, 4H; H_k), 3.25 (t, J = 7.7 Hz, 4H), 3.11 (t, J = 7.7 Hz, 4H), 2.66 (s, 6H; H_j), 1.87 (m, 4H), 1.54 (m, 4H), 1.41 (m, 4H), 1.38 (m, 4H), 0.92 ppm (t, J = 7 Hz, 6H); ^{13}C NMR ($CDCl_3$, 175 MHz): δ = 164.44, 164.34, 164.30, 162.31, 160.82, 155.57, 155.32, 155.02, 153.93, 153.56, 153.03, 149.95, 149.76, 148.55, 140.49, 139.12, 131.65, 129.33, 128.72, 128.55, 127.66, 125.78, 125.11, 123.88, 123.76, 123.56, 121.45, 116.71, 114.02, 113.78, 99.98, 69.59, 36.74, 35.75, 31.56, 29.69, 29.28, 25.69, 22.64, 21.31, 13.82 ppm; ESI-MS: m/z: [M^{+2}] = 1008.

Electrochemical characterization: Cyclic voltammetry was performed by using an Autolab PGStat 30 equipment. These measurements were made in a low-volume BAS cell. A glassy carbon working electrode (BAS MF-2012) was used after being polished with alumina (0.3 μ) for 1 min, and platinum wire was used as counter electrode. A $Ag/AgNO_3$ electrode was used as a reference. Tetrabutylammonium perchlorate (0.1 M) was used as the supporting electrolyte and acetonitrile as solvent. The samples were purged with argon prior to measurement.

Photophysical characterization: UV/Vis spectra were recorded in a 1 cm path-length quartz cell by using a 845x UV/Vis Agilent spectrophotometer, operating with UV/Vis ChemStation Software. Steady-state luminescence spectra were measured by using a Photon Technology spectrofluorometer, equipped with a lamp power supply (LPS-220B), working at room temperature. The excited-state lifetimes and the transient absorption spectra were measured from fresh solutions, which were degassed by

 © 2010 Wiley-VCH Verlag GmbH & Co. KGaA, Weinheim

nitrogen bubbling for 30 min. The excited-state lifetimes of the molecular wire **6** and compound **1b** were measured in the same setup using a nitrogen-laser/dye-laser/frequency-doubler source (PTI). Transient absorption spectra for complexes **8** and compounds **1** were measured by means of a laser flash-photolysis system based on a pulsed Nd:YAG laser, using $\lambda =$ 310 nm as the exciting wavelength. The single pulses were approximately 10 ns duration and the energy was approximately 15 mJ per pulse. A Lo255 Oriel xenon lamp was employed as the detecting light source. The laser flash-photolysis apparatus consisted of the pulsed laser, the Xe lamp, a 77200 Oriel monochromator, and an Oriel photomultiplier (PMT) system made up of a 77348 PMT power supply. The oscilloscope was a TDS-640 A Tektronix. The excited-state lifetimes were deduced from this technique. The quantum yields of **1a** and **1b** compounds were determined in de-aerated acetonitrile solutions at an excitation wavelength of $\lambda = 310$ nm using Equation (1),

$$\phi_x = \phi_r K_{\mathrm{opt}} \frac{(D/A_{\mathrm{exc}})_x}{(D/A_{\mathrm{exc}})_r} \quad (1)$$

for which the subscript x denotes the **1a** and **1b** compounds for which the quantum yield is to be determined (10^{-6} M in CH_3CN), subscript r refers to the reference substance bisulfate quinoline (10^{-6} M in CH_3CN) for which the luminescence quantum yield is assumed to be 0.98, D is the integrated area under the emission spectrum, and A_{exc} is the absorbance at the exciting wavelength. The quantum yields for complexes **8** and the molecular wire **6** were determined in de-aerated acetonitrile solution by using an integrated sphere (Hamamatsu model C9920–0). The system is made up of an excitation light source, consisting of a xenon lamp linked to a monochromator, an integration sphere, and a multi-channel spectrometer.

Device preparation: The pre-patterned ITO glass plates were extensively cleaned, by using chemical and UV-Ozone methods, just before the deposition of the organic layers. Compounds **1** were used as the single active component in preparing double-layer LECs. A first layer of poly(3,4-ethylenedioxythiophene)/polystyrenesulfonate (PEDOT:PSS) (100 nm) was deposited on top of a patterned ITO substrate to increase the device preparation yield. Compounds **1** were then spin-coated from an acetonitrile solution (20 mg mL^{-1}) incorporating the ionic liquid (IL) 1-butyl-3-methylimidazolium hexafluorophosphate in a 1:1 iTMC/IL molar ratio to yield an 80 nm thick layer. The thickness of the films was determined by using an Ambios XP1 profilometer. The IL helps to enhance the performance level of the LEC device.[44,45] On top of the active layer, the metal cathode (aluminum) was thermally evaporated under high vacuum by using an evaporator integrated into an inert atmosphere glovebox (<0.1 ppm O_2 and H_2O). The base pressure for evaporation was $<1\times 10^{-6}$ mbar. Current density and luminance versus voltage were measured using a Keithley 2400 source meter and a photodiode coupled to a Keithley 6485 picoampmeter by using a Minolta LS100 to calibrate the photocurrent. An Avantes luminance spectrometer was used to measure the EL spectrum. Devices were characterized in inert atmosphere.

Computational details: Density functional calculations (DFT) were completed with the D.02 revision of the Gaussian 03 program package,[46] using Becke's three-parameter B3LYP exchange-correlation functional[47–49] together with the 6-31G** basis set for C, H, F, and N atoms[50] and the "double-ζ" quality LANL2DZ basis set for the Ir element.[51] An effective core potential (ECP) replaces the inner core electrons of iridium leaving the outer core $(5s)^2(5p)^6$ electrons and the $(5d)^6$ valence electrons of Ir^{III}. The geometries of the singlet ground state (S_0) and of the lowest triplet excited states were fully optimized by imposing C_2 symmetry restrictions. The hexyloxy groups of the wire and the methyl groups in the bpy and ppy ligands of the end-capping iTMCs were removed. Triplet states were calculated at the spin-unrestricted UB3LYP level with a spin multiplicity of 3. Geometry optimization of the lowest triplet states T_1 (^{3}B) and T_2 (^{3}A) of compounds **1** was achieved by imposing symmetry restrictions to the wavefunction. Solvent effects were considered within the SCRF (self-consistent reaction field) theory using the polarized continuum model (PCM) approach to model the interaction with the solvent.[52,53] Molecular orbitals were calculated in acetonitrile using gas-phase optimized geometries. Starting from the closed-shell S_0 state, time-dependent DFT (TD-DFT) calculations[54–56] were performed in acetonitrile solution to determine the energies and the electronic nature of the lowest excited triplet states at the ground-state geometry. Vertical electronic excitation energies were determined for the lowest 10 triplet states.

Acknowledgements

This work was supported by the ESF (Eurocores-05SONS-FP-021 and FP7-212942-2, FUNMOLS), the Spanish Ministry of Science and Innovation (MICINN) (MAT2006-28185-E, MAT2007-61584, CSD2007-00010, CTQ2006-14987-C02-02, CTQ2009-08790, and CTQ2008-00795), the Generalitat Valenciana(ACOMP/2009/269), and European FEDER funds. R.D.C. and G.F. acknowledge the support of a FPU grant of the MICINN.

[1] G. Saito, F. Wudl, R. C. Haddon, K. Tanigaki, T. Enoki, H. E. Katz, M. Maesato, *Multifunctional Conducting Molecular Materials*, RSC, Cambridge **2007**.
[2] C. J. Brabec, N. S. Sariciftci, J. C. Hummelen, *Adv. Funct. Mater.* **2001**, *11*, 15.
[3] K. M. Coakley, M. D. McGehee, *Chem. Mater.* **2004**, *16*, 4533.
[4] B. C. Thompson, J. M. J. Fréchet, *Angew. Chem.* **2008**, *120*, 62; *Angew. Chem. Int. Ed.* **2008**, *47*, 58.
[5] J. G. C. Veinot, T. J. Marks, *Acc. Chem. Res.* **2005**, *38*, 632.
[6] Z. H. Kafafi, *Organic Electroluminescence*, CRC Press, Boca Raton, **2005**.
[7] K. Müllen, U. Scherf, *Organic Light Emitting-Devices: Synthesis Properties and Applications*, Wiley-VCH, Weinheim, **2006**.
[8] Z. Li, H. Meng, *Organic Light-Emitting Materials and Devices*, CRC, Boca Raton, **2007**.
[9] Q. Pei, G. Yu, C. Zhang, Y. Yang, A. J. Heeger, *Science* **1995**, *269*, 1086.
[10] V. Balzani, S. Campagna, *Photochemistry and Photophysics of Coordination Compounds I, Vol. 280*, Springer, Berlin, **2007**.
[11] M. S. Lowry, W. R. Hudson, R. A. Pascal, S. Bernhard, *J. Am. Chem. Soc.* **2004**, *126*, 14129.
[12] A. B. Tamayo, S. Garon, T. Sajoto, P. I. Djurovich, I. M. Tsyba, R. Bau, M. E. Thompson, *Inorg. Chem.* **2005**, *44*, 8723.
[13] P. T. Chou, Y. Chi, *Chem. Eur. J.* **2007**, *13*, 380.
[14] A. B. Tamayo, B. D. Alleyne, P. I. Djurovich, S. Lamansky, I. Tsyba, N. N. Ho, R. Bau, M. E. Thompson, *J. Am. Chem. Soc.* **2003**, *125*, 7377.
[15] J. D. Slinker, J. Rivnay, J. S. Moskowitz, J. B. Parker, S. Bernhard, H. D. Abruña, G. G. Malliaras, *J. Mater. Chem.* **2007**, *17*, 2976.
[16] J. Slinker, D. Bernards, P. L. Houston, H. D. Abruña, S. Bernhard, G. G. Malliaras, *Chem. Commun.* **2003**, 2392.
[17] J. C. deMello, N. Tessler, S. C. Graham, R. H. Friend, *Phys. Rev. B* **1998**, *57*, 12951.
[18] J. D. Slinker, J. A. DeFranco, M. J. Jaquith, W. R. Silveira, Y. Zhong, J. M. Moran-Mirabal, H. G. Graighead, H. D. Abruña, J. A. Marohn, G. G. Malliaras, *Nat. Mater.* **2007**, *6*, 894.
[19] P. Matyba, K. Maturova, M. Kemerink, N. D. Robinson, L. Edman, *Nat. Mater.* **2009**, *8*, 672.
[20] H. J. Bolink, E. Coronado, R. D. Costa, E. Ortí, M. Sessolo, S. Graber, K. Doyle, M. Neuburger, C. E. Housecroft, E. C. Constable, *Adv. Mater.* **2008**, *20*, 3910.
[21] S. Graber, K. Doyle, M. Neuburger, C. E. Housecroft, E. C. Constable, R. D. Costa, E. Ortí, D. Repetto, H. J. Bolink, *J. Am. Chem. Soc.* **2008**, *130*, 14944.
[22] R. D. Costa, E. Ortí, H. J. Bolink, S. Graber, C. E. Housecroft, M. Neuburger, S. Schaffner, E. C. Constable, *Chem. Commun.* **2009**, 2029.

 © 2010 Wiley-VCH Verlag GmbH & Co. KGaA, Weinheim

[23] R. D. Costa, E. Ortí, H. J. Bolink, S. Graber, S. Schaffner, M. Neuburger, C. E. Housecroft, E. C. Constable, *Adv. Funct. Mater.* **2009**, *19*, 3456.
[24] H. C. Su, H. F. Chen, F. C. Fang, C. C. Liu, C. C. Wu, K. T. Wong, Y. H. Liu, S. M. Peng, *J. Am. Chem. Soc.* **2008**, *130*, 3413.
[25] H. C. Su, F. C. Fang, T. Y. Hwu, H. H. Hsieh, H. Chen, G. Lee, S. Peng, K. T. Wong, C. C. Wu, *Adv. Funct. Mater.* **2007**, *17*, 1019.
[26] L. He, L. Duan, J. Qiao, R. Wang, P. Wei, L. Wang, Y. Qiu, *Adv. Funct. Mater.* **2008**, *18*, 2123.
[27] L. He, J. Qiao, L. Duan, G. Dong, D. Zhang, L. Wang, Y. Qiu, *Adv. Funct. Mater.* **2009**, *19*, 2950.
[28] R. D. Costa, F. J. Céspedes-Guirao, E. Ortí, H. J. Bolink, J. Gierschner, F. Fernández-Lázaro, A. Sastre-Santos, *Chem. Commun.* **2009**, 3886.
[29] J. L. Rodríguez-Redondo, R. D. Costa, E. Ortí, A. Sastre-Santos, H. J. Bolink, F. Fernández-Lázaro, *Dalton Trans.* **2009**, 9787.
[30] H. J. Bolink, L. Cappelli, S. Cheylan, E. Coronado, R. D. Costa, N. Lardiés, M. K. Nazeeruddin, E. Ortí, *J. Mater. Chem.* **2007**, *17*, 5032.
[31] H. Rudmann, M. F. Rubner, *J. Appl. Phys.* **2001**, *90*, 4338.
[32] H. Rudmann, S. Shimada, M. F. Rubner, *J. Am. Chem. Soc.* **2002**, *124*, 4918.
[33] J. D. Slinker, A. A. Gorodetsky, M. S. Lowry, J. Wang, S. Parker, R. Rohl, S. Bernhard, G. G. Malliaras, *J. Am. Chem. Soc.* **2004**, *126*, 2763.
[34] C. Rothe, C.-J. Chiang, V. Jankus, K. Abdullah, X. Zeng, R. Jitchati, A. S. Batsanov, M. R. Bryce, A. P. Monkman, *Adv. Funct. Mater.* **2009**, *19*, 2038.
[35] E. S. Handy, A. J. Pal, M. F. Rubner, *J. Am. Chem. Soc.* **1999**, *121*, 3525.
[36] D. W. Thompson, J. F. Wishart, B. S. Brunschwig, N. Sutin, *J. Phys. Chem. A* **2001**, *105*, 8117.
[37] R. D. Costa, F. J. Céspedes-Guirao, H. J. Bolink, F. Fernández-Lázaro, A. Sastre-Santos, E. Ortí, J. Gierschner, *J. Phys. Chem. C* **2009**, *113*, 19292.
[38] CIE, 1933.
[39] The EQE can be calculated by the equation $h = b\phi/2n^2$, in which b is the recombination efficiency, ϕ is the fraction of excitons that decay radiatively, and n is the refractive index of the glass substrate (the factor $1/2n^2$ accounts for the coupling of light out of the device). The b factor depends on the injection characteristics and is equal to unity when both contacts are ohmic. In first approximation, the parameter ϕ should be equal to the quantum yield of these compounds since the EL emission involves the same emitting states than the photoluminescence emission in these devices. For the glass substrate, the n parameter is approximated to 1.5.
[40] J. C. Scott, G. G. Malliaras in *Conjugated Polymers, Vol. 13*, Wiley-VCH, New York **1999**.
[41] C. Atienza, B. Insuasty, C. Seoane, N. Martín, J. Ramey, G. M. A. Rahmand, D. M. Guldi, *J. Mater. Chem.* **2005**, *15*, 124.
[42] M. Nonoyama, *Bull. Chem. Soc. Jpn.* **1974**, *47*, 767.
[43] S. Sprouse, K. A. King, P. J. Spellane, R. J. Watts, *J. Am. Chem. Soc.* **1984**, *106*, 6647.
[44] S. T. Parker, J. Slinker, M. S. Lowry, M. P. Cox, S. Bernhard, G. G. Malliaras, *Chem. Mater.* **2005**, *17*, 3187.
[45] J. D. Slinker, C. Y. Koh, G. G. Malliaras, M. S. Lowry, S. Bernhard, *Appl. Phys. Lett.* **2005**, *86*, 173506.
[46] Gaussian 03, Revision C.02, M. J. Frisch, G. W. Trucks, H. B. Schlegel, G. E. Scuseria, M. A. Robb, J. R. Cheeseman, J. A. Montgomery, Jr., T. Vreven, K. N. Kudin, J. C. Burant, J. M. Millam, S. S. Iyengar, J. Tomasi, V. Barone, B. Mennucci, M. Cossi, G. Scalmani, N. Rega, G. A. Petersson, H. Nakatsuji, M. Hada, M. Ehara, K. Toyota, R. Fukuda, J. Hasegawa, M. Ishida, T. Nakajima, Y. Honda, O. Kitao, H. Nakai, M. Klene, X. Li, J. E. Knox, H. P. Hratchian, J. B. Cross, V. Bakken, C. Adamo, J. Jaramillo, R. Gomperts, R. E. Stratmann, O. Yazyev, A. J. Austin, R. Cammi, C. Pomelli, J. W. Ochterski, P. Y. Ayala, K. Morokuma, G. A. Voth, P. Salvador, J. J. Dannenberg, V. G. Zakrzewski, S. Dapprich, A. D. Daniels, M. C. Strain, O. Farkas, D. K. Malick, A. D. Rabuck, K. Raghavachari, J. B. Foresman, J. V. Ortiz, Q. Cui, A. G. Baboul, S. Clifford, J. Cioslowski, B. B. Stefanov, G. Liu, A. Liashenko, P. Piskorz, I. Komaromi, R. L. Martin, D. J. Fox, T. Keith, M. A. Al-Laham, C. Y. Peng, A. Nanayakkara, M. Challacombe, P. M. W. Gill, B. Johnson, W. Chen, M. W. Wong, C. Gonzalez, J. A. Pople, Gaussian, Inc., Wallingford CT, **2004**.
[47] A. D. Becke, *J. Chem. Phys.* **1988**, *88*, 2547.
[48] C. T. Lee, W. T. Yang, R. G. Parr, *Phys. Rev. B* **1988**, *37*, 785.
[49] A. D. Becke, *J. Chem. Phys.* **1993**, *98*, 5648.
[50] M. M. Francl, W. J. Pietro, W. J. Hehre, J. S. Binkley, M. S. Gordon, D. J. Defrees, J. A. Pople, *J. Chem. Phys.* **1982**, *77*, 3654.
[51] P. J. Hay, W. R. Wadt, *J. Chem. Phys.* **1985**, *82*, 299.
[52] C. S. Cramer, D. G. Truhlar, *Solvent Effects and Chemical Reactivity*, Kluwer, Dordrecht **1996**.
[53] J. Tomasi, M. Persico, *Chem. Rev.* **1994**, *94*, 2027.
[54] C. Jamorski, M. E. Casida, D. R. Salahub, *J. Chem. Phys.* **1996**, *104*, 5134.
[55] M. Petersilka, U. J. Gossmann, E. K. U. Gross, *Phys. Rev. Lett.* **1996**, *76*, 1212.
[56] M. E. Casida, C. Jamorski, K. C. Casida, D. R. Salahub, *J. Chem. Phys.* **1998**, *108*, 4439.

Received: March 8, 2010
Published online: June 25, 2010

 © 2010 Wiley-VCH Verlag GmbH & Co. KGaA, Weinheim